Thermodynamics of stress-induced ferroelastic transitions: Influence of anisotropy and disorder

Pol Lloveras,[1,2] Teresa Castán,[1,2] Marcel Porta,[1,2,3] Antoni Planes,[1,2] and Avadh Saxena[2,3]
[1]*Departament d'Estructura i Constituents de la Matèria, Universitat de Barcelona, Diagonal 647, 08028 Barcelona, Catalonia, Spain*
[2]*Institut de Nanociència i Nanotecnologia, Universitat de Barcelona, Diagonal 647, 08028 Barcelona, Catalonia, Spain*
[3]*Theoretical Division, Los Alamos National Laboratory, Los Alamos, New Mexico 87545, USA*
(Received 24 February 2010; revised manuscript received 23 April 2010; published 7 June 2010)

Stress-induced stress-strain constitutive behavior has been studied in detail in ferroelastic martensites. It has been found that the weights of the long-range anisotropic interactions and of the disorder are important to determine the fine structure of the stress-strain curves. As experiments show, a wide variety of behaviors has been observed. A decrease of anisotropy and/or increase in the disorder results in changes in the temperature range where pseudoplastic and superelastic regimes are observed. Also, a smoothing of the stress-induced ferroelastic transition, accompanied with a decrease in the transition stress and the hysteresis area, is found. However, Clausius-Clapeyron slope has been observed not to depend on the specific values of anisotropy and disorder. This is in general agreement with experimental results in different alloy families, although some particular features differ from those in experiments. Elastocaloric effect has been studied as well. Varying the anisotropy slightly modifies the shape of the entropy change-temperature curve but the magnitude of the entropy change remains essentially constant.

DOI: 10.1103/PhysRevB.81.214105 PACS number(s): 62.20.D−, 64.70.K−, 81.30.Kf, 62.20.fg

I. INTRODUCTION

Martensites exhibiting ferroelastic stress-strain behavior are of technological interest due to the ability of recovering large deformations by means of either the shape-memory effect (SME) or the superelastic behavior.[1] The former has its origin in a ferroelastic phase of zero macroscopic strain due to the twinned microstructure. It consists of a pseudoplastic[1] deformation, which cannot be recovered by unloading but upon heating when the system undergoes the reverse transformation. On the other hand, superelasticity occurs at constant temperature where, upon loading and unloading, the sample transforms forth and back, respectively, thus recovering the initial shape. However, further conditions must be fulfilled by such materials to become actually useful. For instance, both the SME and superelasticity require appropriate temperature and stress ranges within which the transitions take place.

A wide variety of shape-memory alloy (SMA) families has been studied in order to look for appropriate materials. Moreover, doping has been observed to substantially modify the stability regimes of a given SMA. It turns out to be a good way to explore and identify new regions of the phase space that are likely to be of technological interest. As an example, in $Ti_{50-x}Ni_{50+x}$, the temperature separating superelastic and pseudoplastic regimes decreases drastically when composition is varied from[2] $x=0.6$ to[3] $x=1.5$. Similarly, many other alloys such as Au-Cd,[4] Ti-Ni-Cu,[5] Ni-Mn-Ga,[6] Ni-Co-Mn-In,[7] etc., have been observed to exhibit changes in hysteresis area, percentage of strain recovery, temperature regimes, and particular shape of the stress-strain curves when varying the relative concentration of the constitutive elements. Interestingly, recent research[8,9] has been focused on exploring different compositions of some alloys [in particular, of Ti-Ni-(Cu,Pd,Pt,Au)] to find the specific composition that shows the smallest hysteresis width, which is of technological interest.

All these result in a rich landscape of stress-strain behaviors. However, they share the same grounds, which are intimately linked to the underlying multidomain microstructure (twinning) arising from the well-known self-accommodation process. This mechanism often has a well-localized origin [for instance, a phase boundary (habit plane) or a domain boundary] and spreads out in the bulk due to long-range elastic interactions. The latter emerge from a nondisruptive,[1] knock-on[10] effect that attempts to fit in a coherent manner the new geometries of all the unit cells that result from the structural transition. Consequently, these interactions depend on the specific crystal symmetries and therefore may be highly anisotropic, thus determining the shape of the domain walls. Indeed, linear elasticity relates the weight of the long-range interactions with elastic anisotropy $\mathcal{A}$. In particular, for a cubic system, it is defined as $\mathcal{A}=C_{44}/C'$, where C_{44} and C' denote elastic constants related to shear and deviatoric stresses.

The SME has been an object of extensive modeling effort. Falk[11] was the first to address the modeling of SME by means of the Landau theory. Since then, further Landau-based extensions have been developed to account for diverse aspects of the SME. A three-dimensional Landau model including more realistic, inertial dynamics as well as the strain as the control variable by means of a multiple order-parameter free energy has focused on the dynamical evolution of strain-induced stress-strain behavior.[12] Another quite refined phase-field Landau model allows for a quantitative characterization of stress-strain relations by means of all temperature-dependent thermomechanical properties of both phases such as second- and third-order elastic constants, transformation strain independent of stress and temperature, and weak temperature dependence of hysteresis.[13] Alternatively, the theory of microelasticity[14] has also been used to study, for instance, stress-strain behavior in polycrystalline materials[15] and the ferromagnetic SME.[16] Other models have also been focused on diverse aspects of the SME.[17–19] In the present study, we have chosen a simple Ginzburg-Landau-

based model used in Ref. 20 (and described in Sec. II) which includes all the symmetry-adapted strains because it makes explicit the long-range anisotropic interactions favoring diagonal domain boundaries. Thus, we can control the strength of such interactions which depend strongly on the elastic anisotropy factor $\mathcal{A}$.

Effects of heterogeneities in SMA have also been approached from different points of view. In Ref. 21, the spatial variation of either the stress field of defects or chemical driving force accounts for athermal friction in the evolution of stress-induced martensitic variants. Another inhomogeneous effect, the dynamic tweed, has been addressed by means of thermal fluctuations.[10] Pretransitional static tweed[20] has been obtained by a spatially random, fluctuating field coupling to the order parameter through the harmonic coefficient. This method has also succeeded in modeling of pretransitional mottled structures and anomalies in response functions.[22] This is supported by the high sensitivity of the transition temperature on the specific composition observed in many SMAs together with the consideration of intrinsic compositional fluctuations, which in turn may be enhanced through doping. We employ this method in our model to account for disorder effects.

In this work, we analyze the effect of anisotropy and disorder in stress-induced transitions in ferroelastic martensites. It is found that anisotropy and disorder are relevant in determining the specific shape of the stress-strain curves. Variations in their values result in changes in the transition stress, hysteresis area, transition dynamics, and temperature ranges where pseudoplastic and superelastic regimes are observed (Sec. III A). These results are in rather general qualitative agreement with experiments in Ni-Co-Mn-In (Ref. 7) and Ni-Mn-Ga (Ref. 6) when moving away from the stoichiometry and also with some aspects of experimental results in Ti-Ni,[2] Ti-Ni-Cu,[5] and Au-Cd.[4] However, some other aspects differ from those experimentally observed in these alloy families. From the influence of temperature on the stress-strain curves, we have estimated the elastocaloric effect in these materials which is the mechanical analog of the magnetocaloric effect in magnetic materials. These results are presented in Sec. III B. Finally, in Sec. IV, we discuss our main results.

II. MODEL

Within a Ginzburg-Landau framework, a triple well free-energy density f_{GL} is used to model a first-order martensitic transition, with the deviatoric strain e_2 as the order-parameter (OP) accounting for a two-dimensional square-to-rectangular unit-cell transformation. Mathematically, this is expressed as

$$f_{GL}(\vec{r}) = \frac{\alpha_T}{2}(T - T_c)e_2^2(\vec{r}) - \frac{\beta}{4}e_2^4(\vec{r}) + \frac{\gamma}{6}e_2^6(\vec{r}) + \frac{\kappa}{2}|\nabla e_2(\vec{r})|^2.$$

Here, α_T, κ and T_c are set to unity to define the reduced units. The resulting unit of length l_0 is, in physical units, $l_0 \simeq 0.24$ nm. Then, the remaining model parameters take the following values: $\beta = 1000\kappa/l_0^2$ and $\gamma = 4.86 \times 10^5 \kappa/l_0^2$.

The disorder required to induce heterogeneous effects is introduced as a random variable η via an additional local coupling to the harmonic term. Specifically, $f_\eta(\vec{r}) = \frac{\alpha_T}{2}\eta(\vec{r})e_2^2(\vec{r})$, where $\eta(\vec{r})$ is spatially exponentially pair correlated with a correlation length of ξ and Gaussian distributed with standard deviation[23] ζ. Disorder effects will be taken into account by modifying the value of ζ. Variations on ξ have been checked not to cause any qualitative difference in the results and hence we will set $\xi = 20l_0$.

The coherent matching of the cells may lead to non-OP, symmetry-allowed strain contributions e_1 and e_3, standing for bulk and shear strains, respectively, that here are taken up to the harmonic term in the free energy. By means of the Saint-Vénant compatibility equation[24] and energy minimization, this term gives rise to an additional OP harmonic contribution consisting of a dipolelike integral expression that reflects its long-range character. It turns out to be local in Fourier space, that is, $f_{\text{non-OP}}(\vec{k}) = V(\vec{k})|e_2(\vec{k})|^2$, where the kernel $V(\vec{k})$ takes the following form:[20]

$$V(\vec{k}) = \frac{C_{44}}{2}\frac{(k_x^2 - k_y^2)^2}{Rk^4 + 8(k_x k_y)^2}.$$

Here, $R = C_{44}/(C_{11} + C_{12})$ is the ratio between shear and bulk moduli. The $(k_x^2 - k_y^2)^2$ term easily explains the preferred diagonal directionality of the domain (twin) walls and its coefficient C_{44} directly relates the strength of the potential to the elastic anisotropy factor $\mathcal{A}$ since, at constant temperature T, both are proportional. It shows that, indeed, anisotropy enhances long-range anisotropic interactions. Thus, variations on $\mathcal{A}$ will be introduced by modifying the value of C_{44}. We now analyze the effect of variations of the ratio R, which appears in the denominator of the kernel $V(\vec{k})$. In Fig. 1, we plot $V(\vec{k})$ for two different values of R: (a) $R = 5$ and (b) $R = 0.05$, with $C_{44} = 0.5$ in both cases. It can be seen that the structure of the potential remains robust with respect to changes in this factor. However, as R decreases, the decay in the off-diagonal directions becomes more abrupt since the value of the kernel increases. Notice the significant difference in the vertical scale. It means that, for a given value of the weight C_{44}, (diagonal) tweed textures and twin boundaries are favored more and more as the value of the factor R is decreased. As seen, this also occurs when, for a given value of R, the value of C_{44} is increased. This has been further checked with simulations with different values of this ratio, which are not shown here. Consequently, variations in the factor R do not lead to qualitatively new results. We therefore perform the present study only as a function of the parameter C_{44} and keeping R constant and equal to $R = 0.5$.

The total free energy can be then written as

$$F_T = \int (f_{GL} + f_\eta + f_\sigma)d\vec{r} + \int f_{\text{non-OP}}\, d\vec{k}, \qquad (1)$$

where we have also introduced the effect of an applied external stress field σ, performed by the term $f_\sigma(\vec{r}) = -\sigma e_2(\vec{r})$. The size of simulation cell is $L = 10^3 l_0$, discretized on a 512×512 mesh and subjected to periodic boundary conditions. Purely relaxational dynamics is used to obtain stabilized configurations.

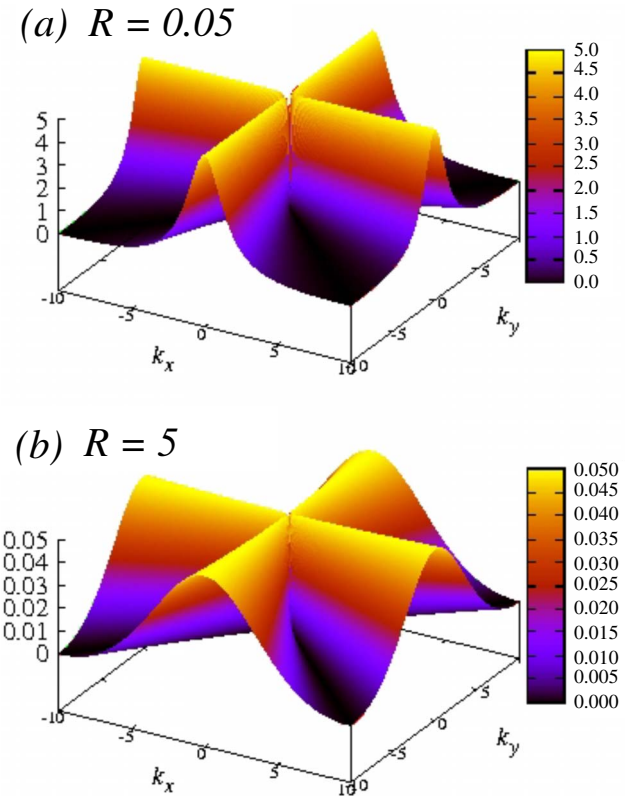

FIG. 1. (Color online) Kernel of the non-OP free-energy density $V(\vec{k})$ for two different values of the ratio $R=C_{44}/(C_{11}+C_{12})$: (a) $R=0.05$ and (b) $R=5$. Here, $C_{44}=0.5$ in both cases. Notice the significant difference in scale.

III. NUMERICAL RESULTS

A. Stress-strain behavior

In this section, we study the thermomechanical behavior of the system when applying and removing an external stress field. In particular, we analyze SME and superelastic behavior.

Since the stress-free stability is crucial for the final unloaded structures, it may be useful to recall the characteristic temperatures that result from a simple stability analysis of the Landau potential. With T_c being the low-stability limit of the high-temperature phase, the equilibrium transition temperature is $T_0=T_c+\frac{3\beta^2}{16\gamma}$ ($\simeq 1.38$) and the high-stability limit of the low-temperature phase $T_i=T_c+\frac{3\beta^2}{4\gamma}$ ($\simeq 1.51$). Taking into account the athermal character of the transition,[25] we expect the system to show pseudoplasticity (which can give rise to SME) below T_i, when the martensite phase is stable or metastable, and superelasticity above T_i, when the martensite phase is unstable. However, in the presence of disorder and considering long-range anisotropic interactions, the transition path determining the stress-strain behavior may be different. We still expect the system to exhibit superelasticity *well* above T_i and pseudoplasticity *well* below T_0, but the stress-strain behavior may be particularly different from the clean-limit scheme in the martensite metastability regime, i.e., $T_0<T<T_i$, and close to it. Thus, we focus the study of the stress-strain behavior in this temperature range.

To illustrate the SME, in Fig. 2, we show the $(\sigma-e_2-T)$ curves obtained for different values of C_{44} ($\sim\mathcal{A}$) and disorder intensity ζ. Case (I) corresponds to $\{C_{44},\zeta\}=\{0.0125,0.13\}$, case (II) to $\{1.135,0.13\}$, case (III) to $\{0.0125,0.04\}$, and case (IV) to $\{1.135,0.04\}$. Arrows in the external margins point toward increasing values of C_{44} and ζ for clarity. The system is first loaded at $T=0.7$ ($<T_c$) until the single-domain state is reached. Then, it is unloaded and finally heated up to a temperature above the transition. In all cases, the curves have been averaged over 50 independent realizations of disorder.[26] Snapshots show representative configurations at a given value of (σ,e_2,T). They have been labeled to make clear the order of the sequence. Focusing on the $(\sigma-e_2)$ curve at $T=0.7$ ($<T_c$), in the four cases, pseudoplasticity is observed. However, each curve exhibits specific peculiarities. When C_{44} ($\sim\mathcal{A}$) is increased and/or the disorder intensity ζ is decreased, the critical stress needed for domain switching increases. The high value of $\mathcal{A}$ [(II) and (IV)] shows initial twinned states whereas low $\mathcal{A}$ values do not allow the system to form twins, but ramified droplets of typical domain size that decreases with[22] ζ. It has been checked that by continuing to increase the disorder, even the highest value of $\mathcal{A}$ is not enough to induce twin formation. It is important to remark that the configuration of low value of $\mathcal{A}$ and high disorder [(I)] exhibits glassy behavior in zero-field (stress)-cooling/field (stress)-cooling simulation experiments.[22] Of course, for all cases upon unloading, the strain is not recovered but the single domain state is maintained since in this temperature regime any ferroelastic variant is stable. However, upon heating, the system undergoes the reverse transformation, ending in a zero net strain and thus recovering the initial macroscopic shape (SME). Some differences are observed between the various heating curves. In fact, they differ in a way analogous to that in the corresponding loading curves mentioned above, from the point of view of sharpness of the profiles.

Figure 3 shows an increasing-T series [(a)–(e)] of stress-strain $(\sigma-e_2)$ curves. For each value of T, the same set of values of anisotropy and disorder of Fig. 2 are used in the corresponding cases (I)–(IV). For a reference framework, the analytical behavior corresponding to the homogeneous Landau free energy is also depicted. Dashed lines correspond to the thermodynamic equilibrium behavior whereas dotted lines denote the maximal metastability regimes. Concerning the temperature evolution of the $\sigma-e_2$ curves, the expected behavior is observed for each case. Pseudoplasticity is observed at low T and then it evolves toward the superelastic regime when T is increased.

Regardless of the differences due to temperature regimes, several common features can be extracted. (i) Case (IV) shows a sharp, clean stress-induced transition whereas in (I), the transition takes place smoothly and gradually. (II) and (III) exhibit intermediate behavior. (ii) In (I) and (IV), pseudoplasticity is observed up to temperatures higher than in (II) and (III), although the underlying behaviors are very different. (iii) (IV) shows the highest transition stress whereas the lowest is observed in (I). (II) and (III) show similar intermediate values. (iv) In the superelastic regime, the backward transition occurs at lower stresses in (IV) than in the other cases. This, combined with (iii), results in a high

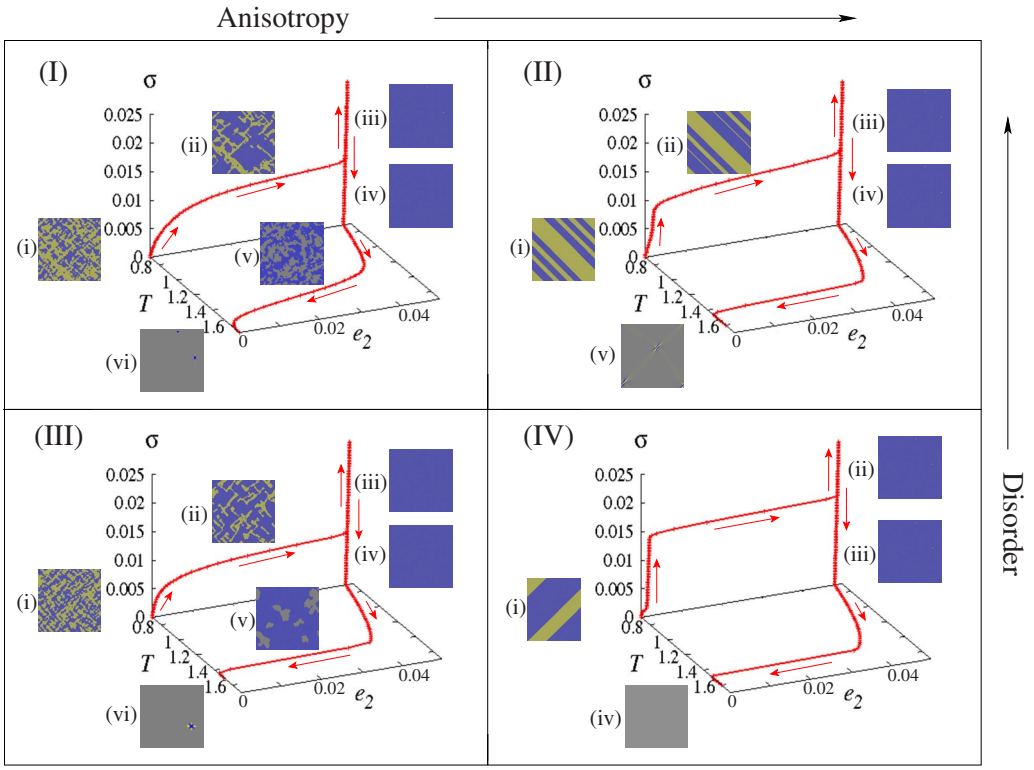

FIG. 2. (Color online) Stress-strain-temperature curves for different values of $C_{44}(\sim\mathcal{A})$ and disorder intensity ζ, giving rise to the SME. The SME can be appreciated in the fact that the initial and final net strains are equal (i.e., both vanish), although the internal microstructure is essentially different. We recall that the characteristic temperatures are $T_c=1$, $T_0\simeq 1.38$, and $T_i\simeq =1.51$.

hysteresis area in (IV) and lower ones for the other cases. From all these, it can be remarked that the effect of decreasing anisotropy (from right to left) is similar to an increase in the disorder (from down to up), which is consistent with the results obtained in Ref. 22. Actually, all these trends are intimately related, as will be discussed in Sec. IV.

Figure 4 displays the transition stresses, σ_t, as a function of temperature (linked symbols).[27] At high temperatures, where superelasticity is observed, σ_t corresponds to the required level of stress for the ferroelastic transition to occur. The relation between σ_t and T is described, in general, by the Clausius-Clapeyron equation. In particular, in all cases, we obtain a linear dependence, which is indeed experimentally observed in martensites.[2–4,6,28–30] Straight lines of constant slope of 0.5 are displayed for comparison between different cases. Nevertheless, it is observed that increasing the amount of disorder or lowering anisotropy results in lower transition stresses, as mentioned above. When the transition temperature is approached, the slope of the curve decreases. Below the transition, the yielding stress, σ_y, does not induce a transition but it is responsible for the domain-wall motion and growth of the selected martensitic variant. It is observed that σ_y increases with decreasing temperature, also in qualitative agreement with experiments.[2–4,28,29] These different regimes occur due to the Landau contribution in the free energy. The presence of long-range interactions and disorder does not modify this general picture but introduces specific ways for the system to behave. For comparison, the σ_t corresponding to the Landau global minimum is depicted with a dashed line whereas the σ_t corresponding to the maximum metastability regime is represented by a dotted line. As can be seen, the slopes of the curves in both Clausius-Clapeyron and pseudoplastic regimes approximate well to the maximal metastability regime than to the equilibrium one.

Figure 5 qualitatively displays the different stress-strain regimes in the parameter space (temperature, anisotropy, disorder), which have been derived from the results in the figures above. Nontrivial behavior is obtained. The dark gray and white regions correspond to the superelastic and pseudoplastic regimes, respectively. In the region in-between (light gray), partial strain recovery is obtained. As can be seen, for large $\mathcal{A}$ and low disorder [(IV) in $\sigma-e_2$ curves], this light gray region is very small.[31] Indeed, the system exhibits either pure pseudoplasticity or pure superelasticity. If we now increase the disorder intensity [(II)] or decrease $\mathcal{A}$ [(III)], the system starts to exhibit (partial) superelasticity in a region where pseudoplasticity was obtained previously [i.e., in (IV)]. However, if we now proceed to decrease $\mathcal{A}$ and increase the disorder simultaneously, the partial superelastic region spreads out into both the previous pseudoplastic and pure superelastic regions.

The largest superelastic regime is achieved when disorder and anisotropy have *comparable* strength, i.e., neither dominates the other but the behavior is the result of a situation of a balance between both factors. In the simulation results, it is observed when anisotropy and disorder values are either both low or both high, as can be seen in Fig. 5 and, more specifically, in (II) and (III) of Fig. 3.

In short, disorder may shift the superelastic regime either to higher or lower temperatures depending on the strength of

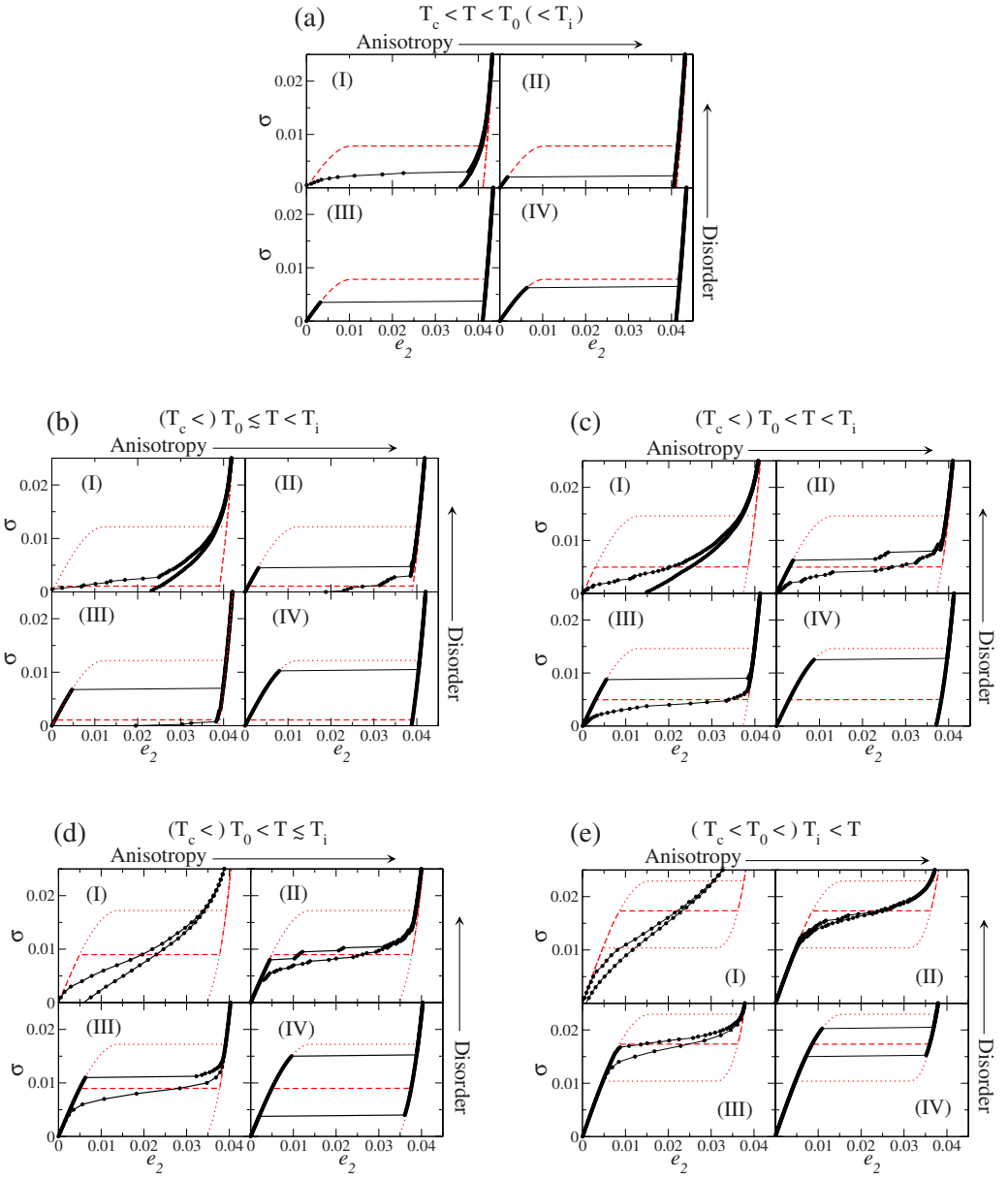

FIG. 3. (Color online) Stress-strain curves for different values of $C_{44}(\sim\mathcal{A})$ and disorder intensity ζ in different temperature regimes.

the elastic anisotropy factor, and conversely. This results in a wide range of mechanical responses, which, interestingly, is also observed experimentally.

B. Elastocaloric effect

The elastocaloric effect is the mechanical analog of the magnetocaloric effect.[32] It is related to the isothermal change of entropy or to the adiabatic change of temperature that takes place in the system when an external stress is applied or removed. As in the magnetocaloric case, large effects are expected in the vicinity of first-order phase transitions where large entropy changes occur.[30] Here, the study of the elastocaloric effect is interesting since it summarizes the information related to the temperature dependence of stress-strain behavior. It has been quantified by means of an isothermal stress-induced entropy change which has been computed from the $\sigma - e_2$ curves[33] as

$$\Delta S(0 \to \sigma) = \int_0^\sigma (\partial S/\partial\sigma) d\sigma$$

$$= \int_0^\sigma (\partial e_2/\partial T) d\sigma$$

$$\simeq \frac{1}{\Delta T}\left\{\int_0^\sigma e_2(T+\Delta T,\sigma) d\sigma - \int_0^\sigma e_2(T,\sigma) d\sigma\right\}. \tag{2}$$

It should be noted that for an ideal first-order transition occurring in equilibrium, this entropy change should coincide with the difference of entropy between the two phases. Here,

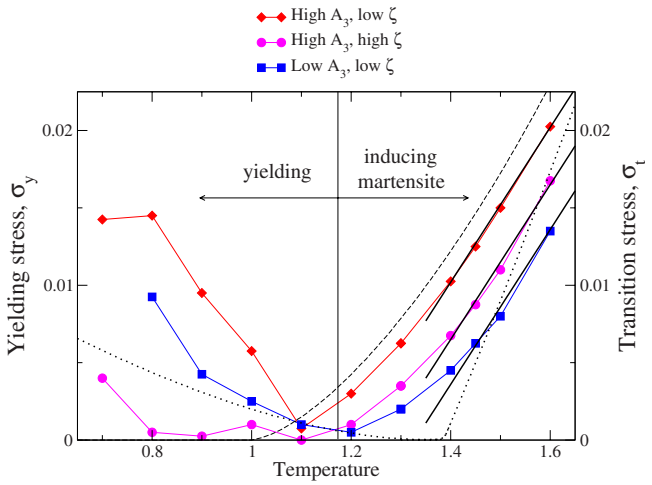

FIG. 4. (Color online) Symbols: transition (right) and yielding (left) stresses as a function of temperature for different values of anisotropy and disorder. Straight lines with same slope are guide to the eyes. Dashed and dotted lines correspond to equilibrium and maximum metastability regimes of the Landau contribution to the free energy.

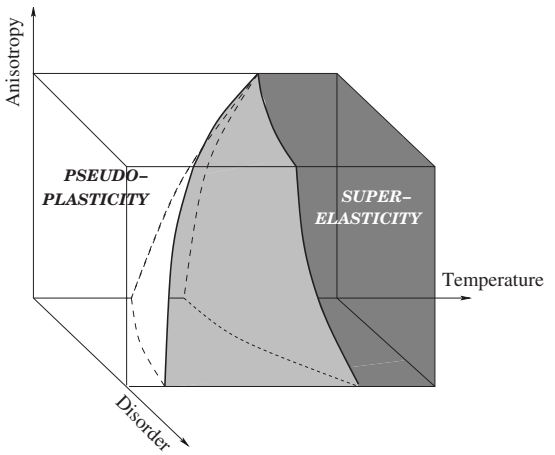

FIG. 5. Different mechanical regimes of the system expressed schematically in the parameter space (temperature, anisotropy, disorder).

due to the existence of disorder, the transition extends over a broad range. Therefore, the obtained behavior will differ from this simple behavior.

Simulation results are shown in Fig. 6. Although the $\sigma - e_2$ curves of the two cases are significantly different (as can be appreciated in Fig. 3), the resulting stress-induced entropy change is similar. The peaks are placed in different positions and the tails show different behavior but the area under the curve remains essentially constant as expected. Moreover, the Landau contribution to the free energy is represented by a dashed line. As can be seen, the presence of disorder (both continuous lines) results in a rounding and decrease of the peak with respect to the Landau contribution.

IV. DISCUSSION

Often, long-range and local effects compete and have opposite consequences. The former contributes to the cohesion of the system by correlating different remote sites of the lattice. Instead, the latter often tries to screen the former and to split the system into uncorrelated pieces. In that sense, high anisotropy values (that increase the strength of the long-range interactions) and/or low disorder favor the stability of each of the thermodynamic phases. It results in a sudden, sharp transition, as it is revealed by the flat plateau in the $(\sigma - e_2)$ curves in Fig. 3. Also, in the paraelastic (i.e., austenite) phase, the larger the anisotropy and/or the lower the disorder, the larger the critical stress field needed to overcome such interactions and thus to carry out the ferroelastic transition. The opposite holds for the reverse transition: as already mentioned, the larger the anisotropy values and/or the lower the disorder, the more stable is the ferroelastic phase and hence, the lower the level of stress at which the system transforms back to the austenite. From this, it follows that there are two main consequences: first, large values of anisotropy and/or low values of disorder result in a larger hysteresis area. Second, the pseudoplastic behavior is observed at higher temperatures.

On the other hand, low values of anisotropy and/or high values of disorder result in a decoupling of the different parts of the system, which may behave uncorrelated from each other. Consequently, the stability becomes short-ranged and the notion of a phase stability for the whole system does not have a meaning anymore. We then observe a set of different, independent critical stresses acting in well-defined regions, i.e., a spatial distribution of critical stresses. It leads to a gradual, smooth transition of the system that starts with the lowest critical stress, corresponding to the transformation of the most unstable region. By increasing the stress field, the system keeps on transforming progressively in moderately stable regions and finishes with the highest critical stress that transforms the most stable zone. Hence, it is not unusual that, at a given temperature, some regions whose stress-free paraelastic stability is weak—or even metastable—may remain anchored in the ferroelastic phase when the stress field is completely removed, either in a weakly stable or metastable state. This is the reason why the total strain is not fully but only partially recovered.

Doping entails atomic disorder so that the translational symmetry of the crystal is broken. As mentioned in Sec. I, it is likely that this may affect any property of a given material. Therefore, it is not unreasonable to think of it as leading to a mesoscopic spatial distribution of characteristic temperatures, i.e., some kind of disorder. However, it is clear that such a definition is up to now purely phenomenological and its utility is assessed by the success in giving results that are in agreement with experiments. In this sense, such a definition has been widely used and many results support it, e.g., precursor textures,[20,22] anomalies[22,34] in the specific heat as well as in the elastic response, and glassy features. Moreover, the behavior of such a model has been shown to be qualitatively quite robust with respect to the specific functionality of the distribution of temperatures and the pair-correlation function[35] in addition to the correlation length and other parameters.[22] In this case, the model shows that a very rich, nontrivial behavior can be found in the mechanical

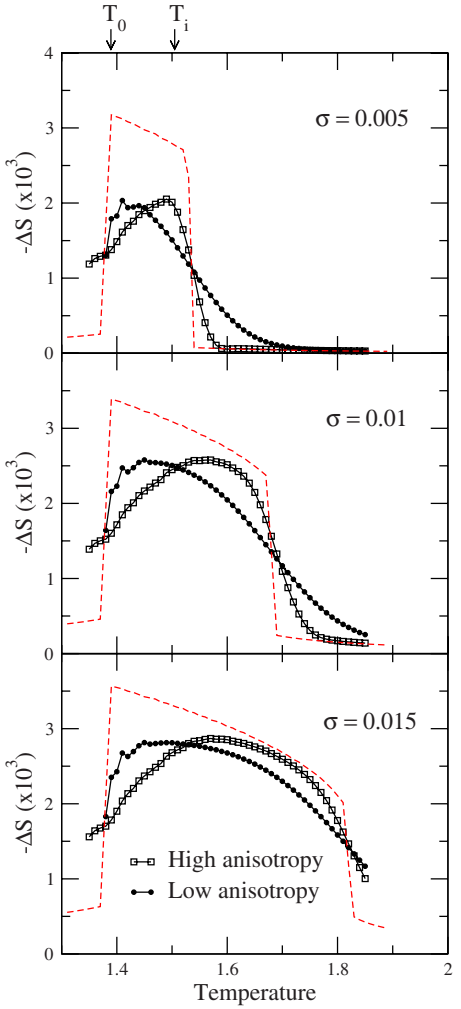

FIG. 6. (Color online) Elastocaloric effect: entropy change as a function of temperature for different values of the applied stress and for different anisotropy values. Dashed line corresponds to the Landau contribution to the free energy.

response as a consequence of the anisotropy and disorder of the system, which can behave in opposite ways depending on the values of these two parameters. Due to the specificities of the model (square symmetry, parameter values, etc.), it becomes difficult to carry out a quantitative comparison between our results and experiments. However, the former show a wide variety of phenomenology that is indeed observed in the latter, thus providing insights for future experimental research. More specifically, for instance, our findings are qualitatively similar to experiments[7] in Ni-Co-Mn-In alloys showing that, at a given temperature, they change from pseudoplastic to partial superelastic and finally to pure superelastic behavior when the In content is increased at the expense of Mn. Ni-Mn-Ga alloys show a shift of the superelastic regime to higher temperatures when doping is increased,[6] which is also consistent with our results. Also, by looking at the experimental results[5] in Ti-Ni-Cu, one can notice that our simulations agree with the decrease in the hysteresis area when Cu content is increased. Nevertheless, the transition stress is observed to increase with Cu content whereas our model shows a decrease of the transition stress when the amount of disorder is increased. Doping has been shown to increase the transition stress also in Ti-Ni when adding off-stoichiometric Ni content.[2,3] Instead, our simulations agree with other strain-induced $\sigma - e_2$ simulations[12] where the transition stress was observed to decrease with the size of a single defect, in accordance with the known fact that defects may act as pinning sites for nucleation and growth of martensite.[36]

Although the magnetocaloric effect is quite different from the elastic analog presented here, very similar Landau-theory-based models have been used to perform simulations in ferromagnetic systems. Such models are known to be sensitive to disorder[37] and dipolar interactions[35] in a similar way to that presented here. For instance, in Ref. 38, it was found that the presence of disorder resulted in a decrease of the magnetocaloric peak, compared to the homogeneous case, which agrees with our results. Encouraged by this, we further emphasize the comparison to magnetocaloric experiments in[39] $Gd_5(Si_xGe_{1-x})_4$, where an increase of x results in a shift of the critical field and the Clausius-Clapeyron slope is approximately independent of doping, which would be consistent with our results.

ACKNOWLEDGMENTS

This work was supported by CICyT (Spain) Project No. MAT2007-61200 and the U.S. Department of Energy. P.Ll. acknowledges support from DGICyT (Spain). We acknowledge fruitful discussions with D. Sherrington.

[1] V. K. Wadhawan, *Introduction to Ferroic Materials* (Gordon and Breach Science Publishers, Amsterdam, 2000).
[2] S. Miyazaki, K. Otsuka, and Y. Suzuki, Scr. Metall. **15**, 287 (1981).
[3] Y. Wang, X. Ren, K. Otsuka, and A. Saxena, Acta Mater. **56**, 2885 (2008).
[4] N. Nakanishi, T. Mori, S. Miura, Y. Murakami, and S. Kachi, Philos. Mag. **28**, 277 (1973).
[5] T.-H. Nam, J.-H. Kim, T.-Y. Kim, Y.-K. Lee, and Y.-W. Kim, J. Mater. Sci. Lett. **21**, 1851 (2002).
[6] V. A. Chernenko, V. L'vov, J. Pons, and E. Cesari, J. Appl. Phys. **93**, 2394 (2003).
[7] R. Kainuma, Y. Imano, W. Ito, Y. Sutou, H. Morito, S. Okamoto, O. Kitakami, K. Oikawa, A. Fujita, T. Kanomata, and K. Ishida, Nature (London) **439**, 957 (2006).
[8] J. Cui, Y. S. Chu, O. O. Famodu, Y. Furuya, J. Hattrick-Simpers, R. D. James, A. Ludwig, S. Thienhaus, M. Wuttig, Z. Zhang, and I. Takeuchi, Nat. Mater. **5**, 286 (2006).
[9] Z. Zhang, R. D. James, and S. Müller, Acta Mater. **57**, 4332 (2009).

[10] A. M. Bratkovsky, S. C. Marais, V. Heine, and E. K. H. Salje, J. Phys.: Condens. Matter **6**, 3679 (1994).
[11] F. Falk, Acta Metall. **28**, 1773 (1980).
[12] R. Ahluwalia, T. Lookman, and A. Saxena, Acta Mater. **54**, 2109 (2006).
[13] V. I. Levitas and D. L. Preston, Phys. Rev. B **66**, 134206 (2002); **66**, 134207 (2002).
[14] A. Artemev, Y. Jin, and A. G. Khachaturyan, Acta Mater. **49**, 1165 (2001).
[15] Y. Jin, A. Artemev, and A. G. Khachaturyan, Acta Mater. **49**, 2309 (2001).
[16] P. P. Wu, X. Q. Ma, J. X. Zhang, and L. Q. Chen, J. Appl. Phys. **104**, 073906 (2008).
[17] K. Tanaka, F. Nishimura, T. Hayashi, H. Tobushi, and C. Lexcellent, Mech. Mater. **19**, 281 (1995).
[18] W. Yan, C. H. Wang, X. P. Zhang, and Y.-W. Mai, Mater. Sci. Eng., A **354**, 146 (2003).
[19] C. Maletta, A. Falvo, F. Furgiuele, and J. N. Reddy, Smart Mater. Struct. **18**, 025005 (2009).
[20] S. Kartha, J. A. Krumhansl, J. P. Sethna, and L. K. Wickham, Phys. Rev. B **52**, 803 (1995).
[21] V. I. Levitas and D.-W. Lee, Phys. Rev. Lett. **99**, 245701 (2007); V. I. Levitas, D.-W. Lee, and D. L. Preston, Int. J. Plast. **26**, 395 (2010).
[22] P. Lloveras, T. Castán, M. Porta, A. Planes, and A. Saxena, Phys. Rev. Lett. **100**, 165707 (2008); Phys. Rev. B **80**, 054107 (2009).
[23] We use ζ notation instead of σ for the standard deviation to avoid confusion with the stress field σ, which will be presented later.
[24] A. Saxena and T. Lookman, in *Handbook of Materials Modeling*, edited by S. Yip (Springer, Berlin, 2005), pp. 2143–2155.
[25] F. J. Pérez-Reche, E. Vives, Ll. Mañosa, and A. Planes, Phys. Rev. Lett. **87**, 195701 (2001).
[26] This allows to obtain a curve with initial vanishing net strain. Otherwise, typically at low temperatures the fractions of the different martensitic variants in a single, twinned configuration are different, which gives rise to a curve with initial nonvanishing net strain.
[27] Not all the $\sigma-e_2$ curves from which the critical stresses have been extracted are shown in this work for clarity.
[28] K. Bhattacharya, *Microstructure of Martensite* (Oxford University Press, Oxford, 2003).
[29] Y. Sutou, N. Kamiya, T. Omori, R. Kainuma, K. Ishida, and K. Oikawa, Appl. Phys. Lett. **84**, 1275 (2004).
[30] E. Bonnot, R. Romero, Ll. Mañosa, E. Vives, and A. Planes, Phys. Rev. Lett. **100**, 125901 (2008).
[31] Let us point out that the origin of the axes does not necessarily correspond to vanishing anisotropy and disorder. Actually, in the limit of no disorder, no partial superelasticity can be observed, i.e., no clear gray area exists. Hence, in the zero-disorder plane, the dashed lines meet, thus removing this region. It has not been done this way since the dependence of the regimes as function of $\mathcal{A}$ for low values of disorder is more clearly depicted as in Fig. 5.
[32] A. M. Tishin, in *Magnetocaloric Effect in the Vicinity of Magnetic Phase Transitions. Handbook of Magnetic Materials*, edited by K. H. J. Buschow (Elsevier Science, Amsterdam, 1998), Vol. 12.
[33] The $\sigma-e_2$ curves used to calculate the elastocaloric effect are not shown here for clarity.
[34] X. Ren, Y. Wang, K. Otsuka, P. Lloveras, T. Castán, M. Porta, A. Planes, and A. Saxena, MRS Bull. **34**, 838 (2009).
[35] M. Porta, T. Castán, P. Lloveras, A. Planes, and A. Saxena, Phys. Rev. B **76**, 054432 (2007).
[36] E. K. H. Salje, *Phase Transitions in Ferroelastic and Co-Elastic Crystals* (Cambridge University Press, Cambridge, England, 1990).
[37] Y. Imry and M. Wortis, Phys. Rev. B **19**, 3580 (1979).
[38] A. Y. Romanov and V. P. Silin, Phys. Met. Metallogr. **83**, 111 (1997).
[39] F. Casanova, A. Labarta, X. Batlle, J. Marcos, Ll. Mañosa, A. Planes, and S. de Brion, Phys. Rev. B **69**, 104416 (2004).